Quantization and Compensation in Sampled Interleaved Multi-Channel Systems

Shay Maymon, *Student Member, IEEE,* Alan V. Oppenheim *Life Fellow, IEEE*

Abstract

This paper considers interleaved, multi-channel measurements as arise for example in time-interleaved analog-to-digital (A/D) converters and in distributed sensor networks. Such systems take the form of either uniform or recurrent nonuniform sampling, depending on the relative timing between the channels. Uniform (i.e. linear) quantization in each channel results in an effective overall signal-to-quantization-error ratio (SQNR) in the reconstructed output which is dependent on the quantizer step size in each channel, the relative timing between the channels and the oversampling ratio. It is shown that in the multi-channel sampling system when the quantization step size is not restricted to be the same in each channel and the channel timing is not constrained to correspond to uniform sampling, it is often possible to reduce the SQNR relative to the uniform case. Appropriate choice of these parameters together with the design of appropriate compensation filtering is developed.

Index Terms

Multi-channel sampling, Recurrent nonuniform sampling, Interleaved A/D, Oversampling, Quantization

I. Introduction

High bandwidth signals or the use of large oversampling ratios often require the use of time-interleaved A/D converters [1]. Similarly in a sensor network environment, separate sensors might independently sample a shifted version of an underlying signal with the sensor outputs then transmitted to a fusion center for interleaving and processing. The relative timing of the channels is typically chosen so that simple interleaving results in uniform sampling. More generally, the interleaved samples correspond to recurrent nonuniform sampling [2–6].

When interleaving is assumed to correspond to uniform sampling but fails to do so because of timing errors, the channel timing is often referred to as mismatched; if not accounted for, this mismatch can lead to significant degradation in performance. A variety of methods have been suggested in the literature to mitigate these problems. To reduce the errors introduced by timing mismatches it is first required to detecting the timing errors. In general, there exist two approaches for detection of timing errors: one which does not assume prior knowledge and is based on the output samples of the time-interleaved A/D converter [7–14], and another which incorporates a known signal at the input to the system [15, 16]. Once the timing errors have been measured, the correction can be done either by adjusting the sampling clock in each A/D converter to eliminate the timing errors, or by digital processing of the output samples to obtain uniform samples.

This work was supported in part by a Fulbright Fellowship, Texas Instruments Leadership University Program, and BAE Systems PO 112991.

In single or multi-channel sampling systems for A/D conversion, quantization effects must also be taken into account. Oversampling is a well established approach to mitigating the effects of quantization, effectively trading off between the oversampling ratio and the required quantization step size for a fixed signal-to-quantization-error ratio. This tradeoff can be accomplished in a direct way by following the quantizer with a sampling rate converter or by using noise-shaping techniques as in delta-sigma A/D converters [17, 18]. A systematic alternative approach is introduced in [19, 20] to derive the time-interleaved equivalent structure for an arbitrary delta-sigma converter. A vector quantization approach is used in [21] to develop a lower bound on the mean squared reconstruction error for periodic bandlimited signals from the quantized oversampled signal. The oversampling technique is further utilized in [22] to reduce the quantization error by modulating the input and the output of the quantizer.

In this paper we consider the effects of uniform quantization in the environment of interleaved, oversampled multi-channel measurements and the design of optimal reconstruction filters[1]. Modeling quantization error with an additive noise model, we show that for the multi-channel case, when the quantizer step size is not constrained to be the same in each channel and the channel timing is not constrained to result in uniform sampling, it is often possible to reduce the SQNR relative to the uniform case. Specifically, we show that timing mismatches between channels can be compensated for by appropriate choice of quantization step size in each channel rather than attempting to correct the timing mismatch. Alternatively, the choice of using different quantizer step size in each channel can be matched by appropriate choice of the relative timing between channels together with properly designed compensation filters. The concept of having different levels of accuracy in different channels is similar to the approach in sub-band coding [23–25] in which each sub-band is quantized with an accuracy based upon appropriate criteria.

The remainder of this paper is organized as follows. Section II introduces the sampling system and discusses perfect reconstruction of the original signal in the absence of errors. In section III uniform quantization is applied to the output samples of the multi-channel system, and the design of optimal reconstruction filters is discussed. Section IV illustrates with examples the optimal choice of the quantizer step size in each channel and the relative timing between the channels. A summary of the results is given in section V.

II. Multi-Channel Sampling and Reconstruction

In this section we introduce the multi-channel sampling system and develop conditions on the reconstruction filters under which perfect reconstruction is achieved in the case of uniform and recurrent nonuniform sampling.

A. Oversampled Multi-Channel System

The basic multi-channel sampling structure which we consider is shown in Figure 1[2] [3]. In this system the Nyquist rate[4] of the bandlimited input signal $x(t)$ is denoted by $1/T_N$, and each of the M channels is sampled at a rate of $1/T = 1/(LT_N)$

[1] A preliminary version of some of this work has been presented in [6].

[2] This system can be viewed as a special case of the more general multi-channel case discussed by Papoulis [4].

[3] Throughout this paper, we use the real-valued variables Ω and ω to denote frequency variables for continuous-time and discrete-time, respectively. Transform-domain signals are denoted with capitalized versions of the time-domain signals, e.g., $X(\Omega)$ and $X(e^{j\omega})$ denote the continuous-time and discrete-time Fourier transforms of $x(t)$ and $x[n]$, respectively, where $e^{j\omega}$ is used to further distinguish between the continuous-time and discrete-time Fourier transforms. Parentheses are used for continuous-time signals and brackets for discrete-time signals.

[4] We refer to the Nyquist rate as the minimum sampling rate required to avoid aliasing, equal to twice the highest frequency contained within the signal.

with $M > L$, corresponding to an effective oversampling factor of $\rho = M/L > 1$. We assume the usual Nyquist-Shannon sampling model but with the sampling done in a multi-channel structure. The notation C/D in Figure 1 represents continuous-to-discrete-time conversion and refers to ideal sampling, i.e., $x_m[n] = x(nT - \tau_m)$ with τ_m as the time delay of the m^{th} channel.

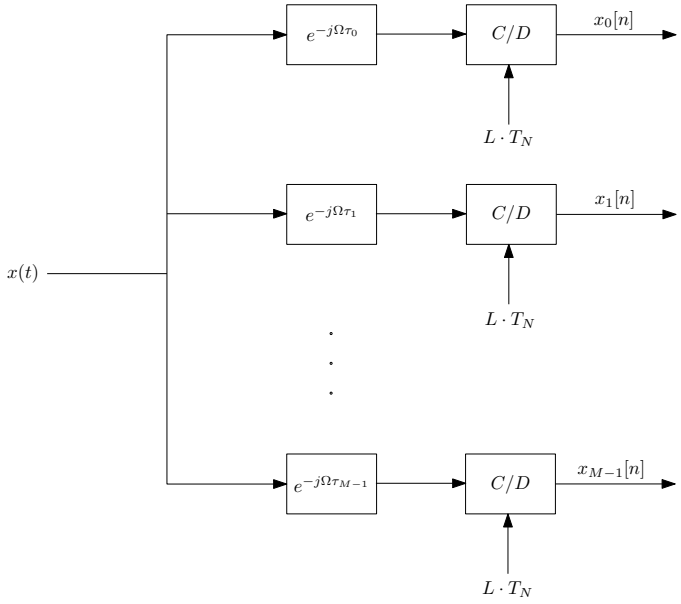

Fig. 1. Multi-channel sampling.

Interleaving the outputs of the multi-channel sampling system, as shown in Figure 2, we obtain either uniform or recurrent nonuniform samples of $x(t)$, depending on the relative timing between the channels. Specifically, when

$$\tau_m = (m/M) \cdot T, \quad m = 0, 1, \ldots, M-1, \tag{1}$$

the interleaved sequence $x_{M/L}[n]$ will correspond to uniform samples of $x(t)$ at a rate of M/L times its Nyquist rate. Otherwise, with nonuniform spacing of the time delays, $x_{M/L}[n]$ will correspond to recurrent nonuniform samples of $x(t)$.

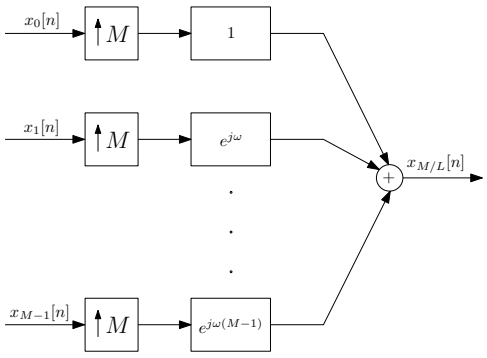

Fig. 2. Interleaving the output samples of the multi-channel sampling system of Figure 1.

B. Perfect Reconstruction

In the absence of errors and when the effective sampling rate of the multi-channel sampling system of Figure 1 meets or exceeds the Nyquist rate of the input signal, perfect reconstruction of $x(t)$ is possible from the multi-channel outputs $\tilde{x}_m[n] = x_m[n]$. For example, perfect reconstruction can be accomplished by combining the sequences $\tilde{x}_m[n]$ through a combination of expanders followed by filters, as shown in Figure 3, to form uniform Nyquist samples of $x(t)$, from which the original continuous-time signal is obtained by sinc interpolation[5].

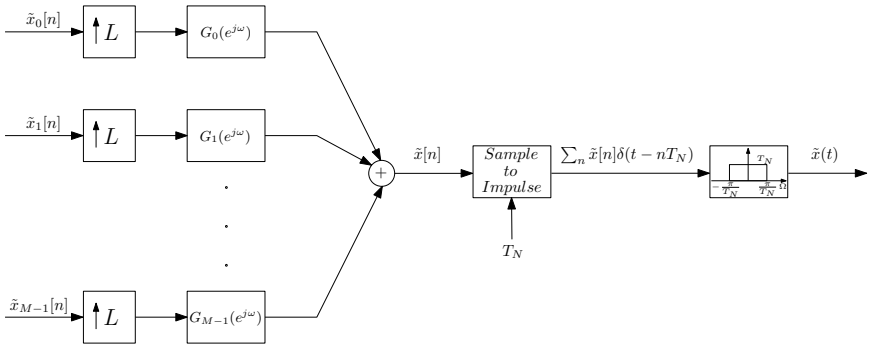

Fig. 3. Multi-channel reconstruction.

When the time delays of the multi-channel system of Figure 1 are uniformly spaced as in (1), choosing the reconstruction filters in the system of Figure 3 as

$$G_m(e^{j\omega}) = \frac{L}{M} e^{j\omega \frac{L}{M} m}, \quad |\omega| < \pi, \quad m = 0, 1, \ldots, M-1, \tag{2}$$

results in perfect reconstruction of $x(t)$. With this choice of $G_m(e^{j\omega})$, the discrete-time processing in the multi-channel reconstruction of Figure 3 is equivalent (see Appendix A) to interleaving, as shown in Figure 2, followed by sampling rate conversion by a noninteger factor of L/M. More generally, the filters $G_m(e^{j\omega})$ are chosen to compensate for the nonuniform spacing of the channel offsets τ_m so that $\tilde{x}[n]$ represents uniform samples of $x(t)$.

Perfect reconstruction of $x(t)$ is obtained in the system of Figure 3 when

$$\sum_{m=0}^{M-1} G_m(e^{j\omega}) \cdot \left[\frac{1}{T} \sum_{k=-(L-1)}^{L-1} X\left(\frac{\omega - \frac{2\pi}{L}k}{T_N} \right) \cdot e^{-j\left(\omega - \frac{2\pi}{L}k\right)\frac{\tau_m}{T_N}} \right] = \frac{1}{T_N} X\left(\frac{\omega}{T_N} \right) \quad |\omega| < \pi. \tag{3}$$

Since the sampling rate in each channel is $1/L$ times the Nyquist rate of the input signal, only L shifted replicas of the spectrum of $x(t)$ contribute to each frequency ω in the spectrum of each signal $x_m[n]$ in Figure 1. Consequently, at each frequency ω, equation (3) imposes L constraints on the M reconstruction filters $G_m(e^{j\omega})$. Of these constraints we impose $L-1$ to remove the aliasing components and one to preserve $X(\Omega)$. Rearranging eq. (3) then results in the following set of

[5]Throughout the paper we refer to convolution of an impulse train of samples with the function $h(t) = \text{sinc}(\frac{\pi}{T_N}t)$ as sinc interpolation and use the historical unnormalized definition of the sinc function, i.e., $\text{sinc}(x) \triangleq \frac{\sin(x)}{x}$.

constraints:

$$\sum_{m=0}^{M-1} G_m(e^{j\omega}) \cdot e^{-j(\omega-\frac{2\pi}{L}k)\tau_m/T_N} = L \cdot \delta[k], \quad \omega \in \Delta\omega_i,$$
$$k = -i, -i+1, \ldots, L-1-i, \quad i = 0, 1, \ldots, L-1, \tag{4}$$

where $\Delta\omega_i = \left[\pi - (i+1)\frac{2\pi}{L}, \pi - i\frac{2\pi}{L}\right]$. When $M = L$, eqs. (4) uniquely determine the reconstruction filters $G_m(e^{j\omega})$. With $M > L$, i.e., with oversampling, there remain $M - L$ degrees of freedom for design of the reconstruction filters. The implications both when $M = L$ and when $M > L$ will be discussed in detail in section III.

If the reconstruction filters in Figure 3 are designed as finite impulse response (FIR) filters, considerable gain in computational efficiency can be achieved by utilizing a polyphase decomposition of $G_m(e^{j\omega})$ and rearranging the operations so that the filtering is done at the low sampling rate.

III. Multi-Channel Sampling and Reconstruction in the presence of quantization error

In this section we consider uniform quantization applied to the multi-channel output samples of Figure 1, i.e., $\tilde{x}_m[n] = Q(x_m[n])$, and we analyze its effect on the reconstructed signal at the output of the system in Figure 3. We design optimal reconstruction filters and provide a lower bound on the output average noise power. The optimal choice of the quantizer step size in each channel and the relative timing between the channels is discussed.

A. Quantization Noise Analysis

In our analysis we represent the error due to the uniform quantizer in each channel through an additive noise model [26–29]. Specifically, the quantizer output $\tilde{x}_m[n]$ in the m^{th} channel is represented as

$$\tilde{x}_m[n] = x_m[n] + q_m[n], \tag{5}$$

where $q_m[n]$ is assumed to be a white-noise process uniformly distributed between $\pm\Delta_m/2$ and uncorrelated with $x_m[n]$, where Δ_m denotes the quantizer step size. Correspondingly, the variance of $q_m[n]$ is $\sigma_m^2 = {\Delta_m}^2/12$.

We denote by $e(t)$ the total noise component in $\tilde{x}(t)$ due to quantization. As shown in Appendix B, $e(t)$ is a zero-mean wide-sense cyclo-stationary random process. The output ensemble average power $E\left(e^2(t)\right)$ of $e(t)$ is also averaged over time to obtain the time and ensemble average power of $e(t)$, denoted σ_e^2 and given by

$$\sigma_e^2 = \frac{1}{T}\int_0^T E(e^2(t))dt = \frac{1}{2\pi}\int_{-\pi}^{\pi} \sum_{m=0}^{M-1} (\sigma_m^2/L) \cdot |G_m(e^{j\omega})|^2 d\omega. \tag{6}$$

B. Optimal Reconstruction Filters

In general, the design of $G_m(e^{j\omega})$ can be formulated in a variety of ways, one of which is to use all degrees of freedom to minimize the reconstruction error [30]. However, in the specific approach taken in this paper, the only characteristic of the signal assumed to be known is its bandwidth. Consequently, we choose the optimal reconstruction filters $G_m(e^{j\omega})$ to minimize σ_e^2 under the set of constraints in (4), which guarantees perfect reconstruction in the absence of error due to quantization. As

shown in Appendix E, the reconstruction filters $G_m(e^{j\omega})$ that minimize σ_e^2 under the set of constraints in (4) are

$$\begin{aligned} G_m(e^{j\omega}) &= 1/\sigma_m^2 \cdot e^{j\omega\tau_m/T_N} \left(\sum_{l=-i}^{L-1-i} \lambda_l^{(i)} \cdot e^{-j2\pi(\tau_m/LT_N)l} \right) \\ &= 1/\sigma_m^2 \cdot e^{j\omega\tau_m/T_N} \cdot \Lambda^{(i)}(e^{j\omega_m}) \qquad (7a) \\ &= 1/\sigma_m^2 \cdot e^{j\omega\tau_m/T_N} \cdot \left(\underline{v}_m{}^H \underline{\lambda}^{(i)} \right) e^{j\omega_m i}, \quad \omega \in \Delta\omega_i \qquad (7b) \\ & \quad i = 0, 1, \ldots, L-1, \quad m = 0, 1, \ldots, M-1, \end{aligned}$$

where $\Lambda^{(i)}(e^{j\omega_m})$ is the discrete-time Fourier transform of the finite-length sequence $\{\lambda_k^{(i)}\}_{k=-i}^{L-1-i}$ sampled in frequency at

$$\omega_m = 2\pi\tau_m/(LT_N) \qquad (8)$$

and

$$\underline{v}_m{}^H = \left[1, e^{-j2\pi\frac{\tau_m}{LT_N}}, \ldots, e^{-j2\pi\frac{\tau_m}{LT_N}(L-1)}\right]. \qquad (9)$$

For each $i = 0, 1, \ldots, L-1$ the sequence $\underline{\lambda}^{(i)} = \{\lambda_k^{(i)}\}_{k=-i}^{L-1-i}$ is defined as the solution to the following set of equations:

$$A_M \cdot \underline{\lambda}^{(i)} = L \cdot \underline{e}_i, \qquad (10)$$

where $\underline{e}_i$ is an indicator vector whose i^{th} entry is 1 and all other entries are zeros, and A_M is an LxL Hermitian Toeplitz matrix such that

$$A_M = \sum_{m=0}^{M-1} (\underline{v}_m \cdot \underline{v}_m{}^H)/\sigma_m^2. \qquad (11)$$

Substituting the expression for $G_m(e^{j\omega})$ from (7a) into (6) we obtain for the minimum achievable value of σ_e^2

$$\sigma_{e\,min}^2 = \frac{1}{L} \sum_{i=0}^{L-1} \left(\frac{1}{L} \sum_{m=0}^{M-1} |\Lambda^{(i)}(e^{j\omega_m})|^2/\sigma_m^2 \right). \qquad (12)$$

Alternatively, using the expression for $G_m(e^{j\omega})$ from (7b), the integrand in eq. (6) can be expressed as

$$\sum_{m=0}^{M-1} (\sigma_m^2/L) \cdot |G_m(e^{j\omega})|^2 = \frac{1}{L} \cdot \left(\underline{\lambda}^{(i)}\right)^H \underbrace{\left(\sum_{m=0}^{M-1} \left(\underline{v}_m \cdot \underline{v}_m{}^H\right)/\sigma_m^2 \right)}_{A_M} \underline{\lambda}^{(i)} = \left(\underline{\lambda}^{(i)}\right)^H \cdot \underline{e}_i, \quad \omega \in \Delta\omega_i, \ i = 0, 1, \ldots, L-1. \qquad (13)$$

Noting that $A_M > 0$ and using (13), an equivalent expression for the minimum value of σ_e^2 becomes

$$\sigma_{e\,min}^2 = \frac{1}{L} \sum_{i=0}^{L-1} \left(\underline{\lambda}^{(i)}\right)^H \cdot \underline{e}_i = \sum_{i=0}^{L-1} \underline{e}_i{}^H A_M^{-1} \underline{e}_i = tr(A_M^{-1}). \qquad (14)$$

When $M = L$, i.e., with no oversampling, it is intuitively reasonable and straightforward to show that the optimal filters in (7) are consistent with the unique solution obtained by solving the perfect reconstruction equations presented in (4). In this

case the impulse response $g_m(t)$ corresponding to the frequency response

$$G_m(\Omega) = \begin{cases} T_N \cdot G_m(e^{j\Omega T_N}) & |\Omega| < \pi/T_N \\ 0 & \text{otherwise} \end{cases}, \quad m = 0, 1, \ldots, M-1, \tag{15}$$

is shown in Appendix C to be

$$g_m(t) = \text{sinc}\left(\frac{\pi}{T}(t+\tau_m)\right) \cdot \left(\prod_{l=0, l\neq m}^{L-1} \frac{\sin\left(\frac{\pi}{T}(t+\tau_l)\right)}{\sin(\frac{\pi}{T}(\tau_l - \tau_m))}\right) \quad m = 0, 1, \ldots, L-1. \tag{16}$$

Consequently, in the absence of error due to quantization and with the reconstruction filters corresponding to $g_m(t)$ in (16), the output $\tilde{x}(t)$ of the system in Figure 3, i.e.,

$$\tilde{x}(t) = \sum_{m=0}^{M-1} \sum_{n=-\infty}^{\infty} \tilde{x}_m[n] \text{sinc}\left(\frac{\pi}{T}(t - nT + \tau_m)\right) \cdot \left(\prod_{l=0, l\neq m}^{L-1} \frac{\sin\left(\frac{\pi}{T}(t - nT + \tau_l)\right)}{\sin(\frac{\pi}{T}(\tau_l - \tau_m))}\right), \tag{17}$$

is a perfect reconstruction of the continuous-time signal $x(t)$. The reconstruction formula in (17) is consistent with [2] and [5]. While the derivation in [5] is based on the Lagrange interpolation formula, the derivation here is carried out by imposing the conditions for perfect reconstruction. As shown in Appendix D, the output average noise power is

$$\sigma_{e,L}^2 = tr(A_L^{-1}) = \frac{1}{L} \cdot \sum_{m=0}^{L-1} \sigma_m^2 \sum_{k=0}^{L-1} \prod_{l=0}^{L-1} \frac{\sin^2(\frac{\pi}{L}(k + \tau_l/T_N))}{\sin^2(\frac{\pi}{LT_N}(\tau_m - \tau_l))}. \tag{18}$$

When $M > L$, eq. (14) together with the Woodbury matrix identity [31] suggest a simple recursive formula for the update of the output average noise power $\sigma_{e_{min}}^2$. Specifically,

$$A_n^{-1} = A_{n-1}^{-1} - A_{n-1}^{-1}\underline{v}_n\underline{v}_n^H A_{n-1}^{-1}/(\sigma_n^2 + \underline{v}_n^H A_{n-1}^{-1}\underline{v}_n) \quad n = L+1, \ldots, M, \tag{19}$$

$$\sigma_{e,n}^2 = tr(A_n^{-1}) = \sigma_{e,n-1}^2 - \frac{\underline{v}_n^H A_{n-1}^{-2}\underline{v}_n}{\sigma_n^2 + \underline{v}_n^H A_{n-1}^{-1}\underline{v}_n} \quad n = L+1, \ldots, M. \tag{20}$$

C. Optimal SQNR in Sampled Interleaved Multi-Channel Systems

In previous sections the effects of quantization in the multi-channel sampling system of Figure 1 were analyzed and optimal reconstruction filters were designed to compensate for the nonuniform spacing of the channel offsets and for the quantization error. It was shown that the effective overall signal-to-noise ratio in the reconstructed output depends on the quantizer step size, the relative timing between the channels and the oversampling ratio. We next discuss how to appropriately choose these parameters for optimal overall SQNR.

Noting that the i^{th} equation in (10) corresponds to

$$\sum_{m=0}^{M-1} 1/\sigma_m^2 \cdot \Lambda^{(i)}(e^{j\omega_m}) = L, \tag{21}$$

and applying the Cauchy-Schwartz inequality to (21) results in

$$\sum_{n=0}^{M-1} 1/\sigma_n^2 \cdot \sum_{m=0}^{M-1} |\Lambda^{(i)}(e^{j\omega_m})|^2/\sigma_m^2 \geq L^2, \tag{22}$$

for each $i = 0, 1, \ldots, L-1$. Combining eqs. (12) and (22) it follows that

$$\sigma_{e_{min}}^2 \geq \frac{L}{\sum_{m=0}^{M-1} 1/\sigma_m^2}, \tag{23}$$

where equality is achieved if and only if the following condition is satisfied

$$\sum_{m=0}^{M-1} 1/\sigma_m^2 \cdot e^{j\omega_m l} = 0 \qquad l = 1, 2, \ldots, L-1. \tag{24a}$$

This condition is equivalent to each of the following conditions:

$$\Lambda^{(i)}(e^{j\omega_m}) = \frac{L}{\sum_{n=0}^{M-1} 1/\sigma_n^2} \qquad \begin{matrix} i = 0, 1, \ldots, L-1 \\ m = 0, 1, , \ldots, M-1, \end{matrix} \tag{24b}$$

$$\lambda_k^{(i)} = \frac{L}{\sum_{m=0}^{M-1} 1/\sigma_m^2}\delta[k] \qquad k = -i, -i+1, \ldots, L-1-i. \tag{24c}$$

When the quantizers in Figure 1 all have the same step size, we next show that τ_m as given by eq. (1) is optimal, i.e., the relative timing between adjacent channels is a constant. The optimal reconstruction filters in (7) then reduce to the noninteger delays in (2). Also in this case,

$$\sigma_{e_{min}}^2 = (L/M) \cdot \sigma^2, \tag{25}$$

where σ^2 denotes the variance of the quantization noise source in each channel. To show this, we note that with $\sigma_m^2 = \sigma^2$, the condition of eq. (24a) becomes

$$\sum_{m=0}^{M-1} e^{j\omega_m l} = 0, \qquad l = 1, 2, \ldots, L-1, \tag{26}$$

which is clearly satisfied for any L and M when the values $e^{j\omega_m}$ are uniformly spaced on the unit circle, corresponding to uniform sampling. However, this is in general not a unique solution as there are other distributions of ω_m which satisfy eq. (26). In summary, it follows from eq. (23) that for the reconstruction structure suggested in Figure 3 and with the quantization step size the same in each channel, the uniform sampling grid achieves the minimum average quantization noise power $(L/M) \cdot \sigma^2$. Any other choice of τ_m, for which (26) is not satisfied, results in a higher average quantization noise power.

As we next show, by allowing the quantization step size to be chosen separately for each channel, so that quantization noise sources $q_m[n]$ in the different channels have different variances σ_m^2, better SQNR can often be achieved. For comparison purposes, we will assume that the quantization noise power averaged over all channels is equal to a pre-specified fixed number σ^2 [6] , i.e.,

$$\frac{1}{M}\sum_{m=0}^{M-1} \sigma_m^2 = \sigma^2. \tag{27}$$

[6]A similar result can be shown if instead of fixing the average power of the quantization noise sources in each of the channels we fix the total number of bits used to quantize the samples.

Applying the Cauchy-Schwartz inequality to the identity $\sum_{m=0}^{M-1} \sigma_m \cdot 1/\sigma_m = M$, it follows that

$$\sum_{m_1=0}^{M-1} \sigma_{m_1}^2 \cdot \sum_{m_2=0}^{M-1} 1/\sigma_{m_2}^2 \geq M^2, \tag{28}$$

and equivalently

$$\frac{L}{\sum_{m=0}^{M-1} 1/\sigma_m^2} \leq (L/M) \cdot \sigma^2, \tag{29}$$

with equality if and only if

$$\sigma_m^2 = \sigma^2 \qquad m = 0, 1, \ldots, M-1. \tag{30}$$

Together with (23), we conclude that by having different levels of accuracy in the quantizers in the different channels, there is the possibility of reducing the average quantization noise power. This suggests a way to compensate for the mismatched timing in the channels of Figure 1 and increase the total SQNR. Alternatively, we can deliberately introduce timing mismatch so that with appropriate design of the quantizers, we will achieve better SQNR as compared to the equivalent uniform sampling with equal quantizer step size in each channel. The analysis and conclusions of course rely on the validity of the additive noise model used for the quantizer, which becomes less appropriate as the quantizer step size increases or the relative timing between adjacent channels decreases.

IV. Simulations

In this section, we consider the multi-channel sampling system of Figure 1 with $M = 3$ and $L = 2$ followed by uniform quantization. Three cases are considered, each corresponding to a different assumption with respect to the relative timing between the channels and the quantization step size in each channel. In the first case, the quantization step size in each channel is fixed and equal in all channels, and the relative timing between channels is optimized. In the second case, the relative timing between the channels is specified, and the bit allocation is optimized subject to a bit-budget constraint. In the third case, each channel is allocated a different number of bits, and the relative timing between channels is optimized to maximize the SQNR.

Figure 4 shows the factor $\gamma = \sigma^2/\sigma_{e_{min}}^2$ representing the reduction in the average noise power for the case of $\sigma_m^2 = \sigma^2 \quad \forall m$ as a result of the reconstruction of Figure 3 with $M = 3$, $L = 2$, and $\tau_0 = 0$. As indicated, the maximum noise reduction is achieved for $\tau_1 = -\tau_2 = \pm(2/3) \cdot T_N$, for which $\sigma_{e_{min}}^2 = (2/3) \cdot \sigma^2$.

It follows from eq. (23) and is illustrated in the preceding example that for the reconstruction structure suggested in Figure 3 and with the quantization step size the same in each channel, the uniform sampling grid achieves the minimum average quantization noise power $(L/M) \cdot \sigma^2$. Any other choice of τ_m for which (26) is not satisfied results in a higher average quantization noise power.

We next illustrate with an example that with appropriate design of the quantizer in each channel we can compensate for the mismatched timing in the channels of Figure 1. With 4-bit uniform quantizers in each of the channels, it follows from eq. (14) that when the time delays are $\tau_0 = 0$, $\tau_1 = T_N/8$ and $\tau_2 = -(3/4)T_N$, the output average noise power is increased by approximately 20% relative to the case where $\{\tau_m\}$ are chosen according to (1). However, when the quantizer step size is not

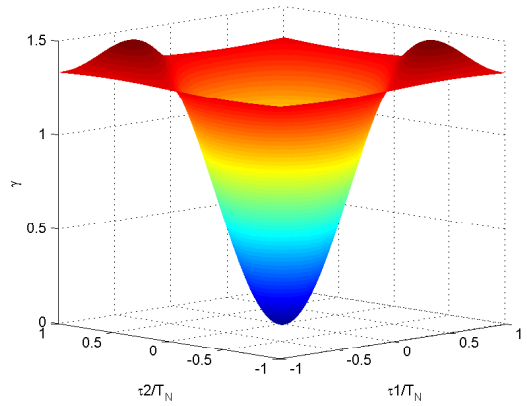

Fig. 4. The reduction factor γ in the average noise power at the output of the reconstruction of Figure 3 achieves its maximum value at $\tau_1 = -\tau_2 = \pm(2/3)\cdot T_N$, i.e., when the multi-channel sampling is equivalent to uniform sampling. Since this curve is based on the additive noise model of the quantization error, which assumes uncorrelated errors, it is less accurate in the vicinity of $\tau_1 = 0$, $\tau_2 = 0$ and $\tau_1 = \tau_2$.

constrained to be the same in each channel, the reconstruction error variance can be reduced. Table I shows the performance gain for different bit allocations as compared to the case in which each channel is allocated 4 bits. The results are sorted from the most to the least preferable where in each choice only 1 bit is shifted from one channel to another, keeping the total number of bits the same.

In general, we might intuitively expect that since the sampling instants of channel 2 are relatively far from those of the other two channels, it should be allocated more bits in compensation. Also, the relative timing between channel 0 and channel 2 is smaller than the relative timing between channel 2 and channel 1, suggesting allocation of more bits to channel 1 as compared to channel 0. This intuition of bit allocation according to the relative timing between adjacent channels is consistent with the results in Table I and in particular with the optimal choice shown in Figure 5, which suggests allocating 3 bits to channel 0, 4 bits to channel 1, and 5 bits to channel 2.

N_0	N_1	N_2	$(\sigma_{e_{min}}^2)_{(4,4,4)}/(\sigma_{e_{min}}^2)_{(N_0,N_1,N_2)}$
3	**4**	**5**	**1.46**
4	3	5	1.36
3	5	4	1.26
5	3	4	1.14
4	5	3	0.41
5	4	3	0.38

TABLE I
THE PERFORMANCE GAIN FOR DIFFERENT BIT ALLOCATIONS

We next fix the number of bits in channel 0 to 3, channel 1 to 4, and channel 2 to 4, and without loss of generality set $\tau_0 = 0$. The values of τ_1 and τ_2 are chosen to minimize the output average noise power. Note that when $\tau_1 = -\tau_2 = \pm(2/3)T_N$, the multi-channel sampling is equivalent to uniform sampling. More generally, solving (24) for the optimal time delays yields the following equation:

$$64 + 256e^{j\omega_1} + 256e^{j\omega_2} = 0, \tag{31}$$

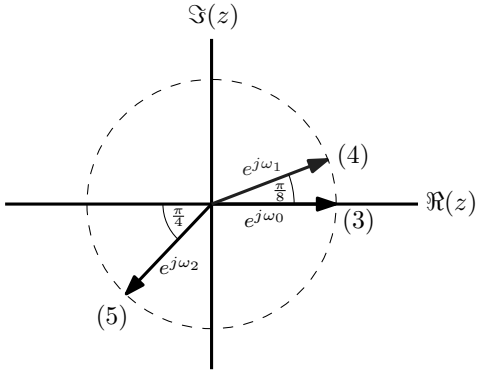

Fig. 5. Each vector represents a channel whose time delay τ_m is determined by the vector's phase ω_m according to the transformation $\omega_m = 2\pi\tau_m/(LT_N)$, which maps the region $\tau_m \in [-T_N, T_N]$ into the region $\omega_m \in [-\pi, \pi]$. The numbers associated with each of the vectors are the optimal bit allocations for the case of $\tau_0 = 0$, $\tau_1 = T_N/8$ and $\tau_2 = -3T_N/4$.

for which $\omega_1 = -\omega_2 = \pm 0.5402\pi$ (corresponding to $\tau_1 = -\tau_2 = \pm 0.5402T_N$) is a solution, as Figure 6 illustrates. Consistent with the intuition expressed earlier, since channels 1 and 2 are both allocated 4 bits and channel 0 is allocated only 3 bits, the optimal choice of τ_1 and τ_2 is such that the relative timing between channel 1 and channel 0, which is equal to the relative timing between channel 0 and channel 2, is much smaller than that between channel 2 and channel 1, compensating for the low accuracy in channel 0. If channel 0 were allocated 4 bits as the other two channels are, the optimal choice of the time delays would have been $\tau_1 = -\tau_2 = \pm(2/3)T_N$, corresponding to uniform sampling; however, since channel 0 is allocated fewer bits than the other two channels, the sampling instants of the other two channels are getting closer to that of channel 0 in compensation. Since this choice of time delays provides the solution to (24), the output average noise power σ_e^2 achieves the lower bound in (23), i.e., $\sigma_e^2 = L/(\sum_{m=0}^{M-1} 1/\sigma_m^2)$.

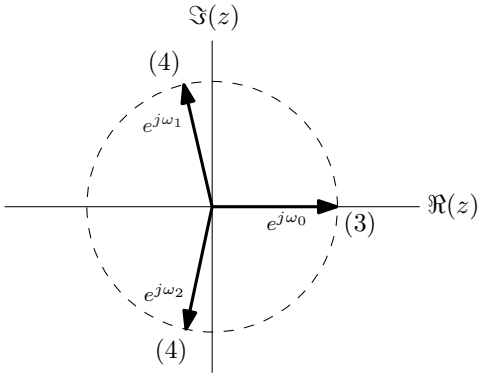

Fig. 6. With bit allocation $N_0 = 3$, $N_1 = 4$, and $N_2 = 4$, the optimal choice of time delays is $\tau_1 = -\tau_2 = \pm 0.5402T_N$, for which the multi-channel sampling system is equivalent to recurrent nonuniform sampling.

Figure 7 shows the relative gain with respect to output average noise power for all values of τ_1 and τ_2 in the range $[-T_N, T_N]$, as compared to the case of uniform sampling. As indicated, an improvement of 12.5% relative to the uniform sampling case is achieved for the optimal choice $\tau_1 = -\tau_2 = \pm 0.5402T_N$.

In summary, we have illustrated that with nonuniform spacing of the time delays, for which the interleaved multi-channel outputs correspond to recurrent nonuniform sampling, equal quantization step size in each channel is not optimal. Allowing different levels of accuracy in the quantizers in the different channels achieves a reduction in the noise variance. Alternatively,

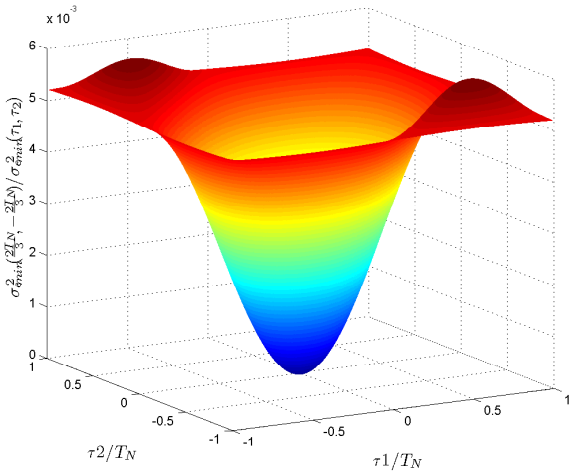

Fig. 7. The relative performance compared to uniform sampling as a function of τ_1 and τ_2 when $\tau_0 = 0$, $N_0 = 3$, $N_1 = 4$, and $N_2 = 4$. Since this curve is based on the additive noise model of the quantization error, which assumes uncorrelated errors, it is less accurate in the vicinity of $\tau_1 = 0$, $\tau_2 = 0$ and $\tau_1 = \tau_2$.

when the quantization step size in each of the channels is fixed and varies among channels, choosing the realtive timing between adjacent channels to be the same is not optimal, and lower average noise power is achieved with nonuniform spacing of the time delays.

V. CONCLUSIONS

In this paper we have considered the effects of uniform quantization in the environment of interleaved, oversampled multi-channel measurements. We have shown that with uniform quantization and equal quantizer step size in each channel, the effective overall signal-to-noise ratio in the reconstructed output is maximized when the multi-channel sampling is equivalent to uniform sampling. With different levels of accuracy in each channel, uniform spacing of the time delays is in general not optimal, and better results can often be achieved with nonuniform spacing corresponding to recurrent nonuniform sampling. Similarly, for the case of nonuniform spacing of the time delays, equal quantization step size in each channel is in general not optimal and a higher signal-to-quantization-noise ratio can be often achieved when allowing different levels of accuracy in the quantizers in the different channels. We have developed the optimal reconstruction filters to minimize the time and ensemble average power of the reconstruction error under the constraints which guarantee perfect reconstruction in the absence of quantization error.

APPENDIX A
MULTI-CHANNEL SAMPLING RATE CONVERSION

Interleaving the outputs of the multi-channel sampling system of Figure 1 and subsequent processing through sampling rate conversion by a noninteger factor of L/M, we obtain the system of Figure A.1.

Interchanging expanders with filtering we obtain the system of Figure A.2, from which it follows that

$$G_m(e^{j\omega}) = \frac{L}{M} e^{j\omega \frac{L}{M} m}, \quad |\omega| < \pi, \quad m = 0, 1, \ldots, M-1. \tag{A-1}$$

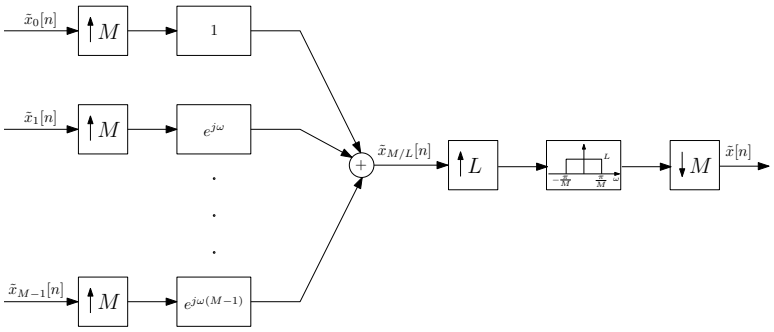

Fig. A.1. Interleaving followed by sampling rate conversion.

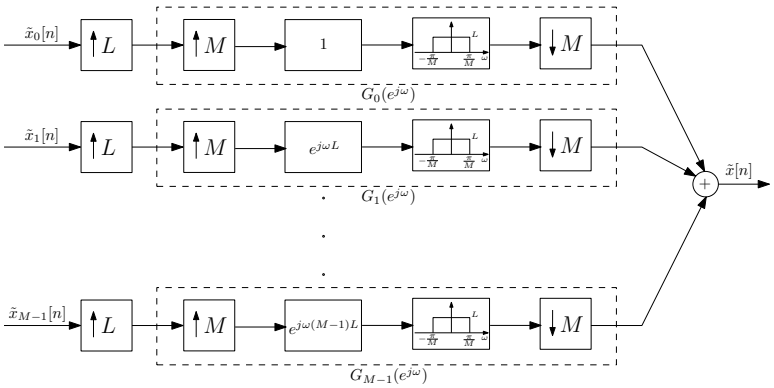

Fig. A.2. Multi-channel sampling rate conversion.

APPENDIX B

THE OUTPUT AVERAGE NOISE POWER DUE TO QUANTIZATION

To analyze the effect of each channel of Figure 3 on the corresponding quantization noise, we consider the system of Figure B.1 whose output $\tilde{q}_m(t)$ is

$$\tilde{q}_m(t) = \sum_{n=-\infty}^{\infty} q_m[n] g_m(t - nT), \tag{B-1}$$

where $g_m(t)$ is the impulse response corresponding to the frequency response

$$G_m(\Omega) = \begin{cases} T_N \cdot G_m(e^{j\Omega T_N}) & |\Omega| < \pi/T_N \\ 0 & \text{otherwise} \end{cases}, \quad m = 0, 1, \ldots, M-1. \tag{B-2}$$

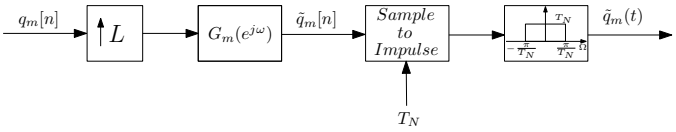

Fig. B.1. A single channel in the reconstruction system of Figure 3.

Under the assumption that $q_m[n]$ is a zero-mean white-noise process with variance σ_m^2, the autocorrelation function of $\tilde{q}_m(t)$

is

$$R_{\tilde{q}_m\tilde{q}_m}(t,t-\tau)=\sigma_m^2\cdot\sum_{k=-\infty}^{\infty}g_m(t-kT)g_m(t-\tau-kT), \tag{B-3}$$

which is periodic in t with period $T=LT_N$ and $\tilde{q}_m(t)$ is therefore a wide-sense cyclo-stationary random process. Alternatively, $R_{\tilde{q}_m\tilde{q}_m}(t,t-\tau)$ can be expressed as

$$R_{\tilde{q}_m\tilde{q}_m}(t,t-\tau)=\frac{1}{2\pi}\int_{-\pi/T_N}^{\pi/T_N}S_{\tilde{q}_m\tilde{q}_m}(\Omega;t)\cdot e^{j\Omega\tau}d\Omega, \tag{B-4}$$

where

$$S_{\tilde{q}_m\tilde{q}_m}(\Omega;t)=\begin{cases}\sigma_m^2\cdot T_N{G_m}^*(e^{j\Omega T_N})\cdot\sum_{k=-\infty}^{\infty}g_m(t-kT)e^{-j\Omega(t-kT)} & |\Omega|<\frac{\pi}{T_N}\\ 0 & \text{otherwise}\end{cases}. \tag{B-5}$$

We denote by $e(t)$ the total noise component in $\tilde{x}(t)$ due to quantization, i.e.,

$$e(t)=\sum_{m=0}^{M-1}\tilde{q}_m(t). \tag{B-6}$$

With the assumption that the quantization noise is uncorrelated between channels,

$$R_{ee}(t,t-\tau)=\sum_{m=0}^{M-1}R_{\tilde{q}_m\tilde{q}_m}(t,t-\tau), \tag{B-7}$$

from which it follows that $e(t)$ is also a wide-sense cyclo-stationary random process. Thus, the ensemble average power $E(e^2(t))$ of $e(t)$ is periodic with period T. Averaging also over time and denoting by σ_e^2 the time and ensemble average power of $e(t)$, we obtain

$$\sigma_e^2=\frac{1}{T}\int_0^T E(e^2(t))dt=\frac{1}{T}\int_0^T R_{ee}(t,t)dt=\sum_{m=0}^{M-1}\frac{1}{T}\int_0^T R_{\tilde{q}_m\tilde{q}_m}(t,t)dt. \tag{B-8}$$

Expressing $R_{\tilde{q}_m\tilde{q}_m}(t,t)$ in terms of $S_{\tilde{q}_m\tilde{q}_m}(\Omega;t)$ as in (B-5), eq. (B-8) becomes

$$\begin{aligned}\sigma_e^2 &= \sum_{m=0}^{M-1}\frac{\sigma_m^2}{2\pi L}\cdot\int_{-\pi/T_N}^{\pi/T_N}{G_m}^*(e^{j\Omega T_N})\cdot\left(\sum_{k=-\infty}^{\infty}\int_0^T g_m(t-kT)e^{-j\Omega(t-kT)}dt\right)d\Omega\\ &= \frac{1}{2\pi}\int_{-\pi}^{\pi}\sum_{m=0}^{M-1}(\sigma_m^2/L)\cdot|G_m(e^{j\omega})|^2d\omega.\end{aligned} \tag{B-9}$$

APPENDIX C
PERFECT RECONSTRUCTION FROM NYQUIST SAMPLES

Writing the equations in (4) in a matrix form, we obtain

$$V\cdot\begin{bmatrix}e^{-j\omega_0 i}\cdot G_0(e^{j\omega})\cdot e^{-j\omega\tau_0/T_N}\\ e^{-j\omega_1 i}\cdot G_1(e^{j\omega})\cdot e^{-j\omega\tau_1/T_N}\\ \ddots\\ e^{-j\omega_{M-1} i}\cdot G_{M-1}(e^{j\omega})\cdot e^{-j\omega\tau_{M-1}/T_N}\end{bmatrix}=L\cdot\underline{e}_i,\quad \omega\in\Delta\omega_i,\ i=0,1,\ldots,L-1, \tag{C-1}$$

where $\underline{e}_i$ is an indicator vector whose i^{th} entry is 1 and all other entries are zeros, and V is an LxM vandermonde matrix of the form

$$V = \begin{pmatrix} 1 & 1 & \dots & 1 \\ \alpha_1 & \alpha_2 & \dots & \alpha_M \\ \alpha_1^2 & \alpha_2^2 & \dots & \alpha_M^2 \\ \dots & \ddots & \ddots & \dots \\ \alpha_1^{L-1} & \alpha_2^{L-1} & \dots & \alpha_M^{L-1} \end{pmatrix} \tag{C-2}$$

with $\alpha_{m+1} = e^{j\omega_m}, \quad m = 0, 1, \dots, M-1$. When $M = L$ and all α_m are distinct, V is invertible. Using the explicit formula in [32] for the inverse of a square vandermonde matrix in solving eqs. (C-1) for the case $M = L$ results in

$$G_m(e^{j\omega}) = L \cdot e^{j\omega_m i} \cdot e^{j\omega\tau_m/T_N} \cdot \frac{(-1)^{L-1-i}}{\prod_{l=0,l\neq m}^{L-1}(\alpha_{m+1} - \alpha_{l+1})} \cdot \sigma_{L-1-i,L-1}^{m+1}, \ \omega \in \Delta\omega_i, \\ i = 0, 1, \dots, L-1, \ m = 0, 1, \dots, L-1, \tag{C-3}$$

where the coefficients $\{\sigma_{L-1-i,L-1}^{m+1}\}_{i=0}^{L-1}$ are determined by the following expansion

$$\prod_{l=1,l\neq m+1}^{L}(x - \alpha_l) = \sum_{i=0}^{L-1}(-1)^{L-1-i}x^i\sigma_{L-1-i,L-1}^{m+1}. \tag{C-4}$$

Denoting by $g_m(t)$ the impulse response corresponding to the frequency response $G_m(\Omega)$ in (15), it follows from eqs. (C-3) and (C-4) that

$$g_m(t - \tau_m) = \frac{1}{2\pi}\int_{-\pi/T_N}^{\pi/T_N} T_N G_m(e^{j\Omega T_N})e^{j\Omega(t-\tau_m)}d\Omega \tag{C-5}$$

$$= \frac{\left(\sum_{i=0}^{L-1}(-1)^{L-1-i}(\alpha_{m+1}e^{-j\frac{2\pi}{LT_N}t})^i \cdot \sigma_{L-1-i,L-1}^{m+1}\right)}{\prod_{l=0,l\neq m}^{L-1}(\alpha_{m+1} - \alpha_{l+1})} \cdot \text{sinc}(\pi t/T) \cdot e^{j\frac{\pi}{T_N}(\frac{L-1}{L})t}$$

$$= \prod_{l=0,l\neq m}^{L-1}\frac{(\alpha_{m+1}e^{-j\frac{2\pi}{LT_N}t} - \alpha_{l+1})}{(\alpha_{m+1} - \alpha_{l+1})} \cdot \text{sinc}(\pi t/T) \cdot e^{j\frac{\pi}{T_N}(\frac{L-1}{L})t}, \quad m = 0, 1, \dots, L-1. \tag{C-6}$$

Substituting $\alpha_{m+1} = e^{j\omega_m}$ in (C-6) results in $g_m(t)$ as given in (16).

APPENDIX D
NYQUIST SAMPLING - THE OUTPUT AVERAGE NOISE POWER

With no oversampling, i.e., when $M = L$, A_L can be represented as

$$A_L = V\Sigma^{-1}V^H, \tag{D-1}$$

where V is given by (C-2) and $\Sigma = diag[\sigma_0^2, \sigma_1^2, \dots, \sigma_{L-1}^2]$. Since V is invertible, the minimum achieved output average noise power can be written as

$$\sigma_{e,L} = tr(A_L^{-1}) = tr(U\Sigma U^H) = \sum_{m=0}^{L-1}\sigma_m^2|\underline{u}_m|^2, \tag{D-2}$$

where $U^H = V^{-1}$ and $\underline{u}_m$ denotes the m^{th} column of U. Using the formula in [32] for the inverse of V in calculating the norm of $\underline{u}_m$, we obtain

$$|\underline{u}_m|^2 = \sum_{i=0}^{L-1} |u_{i,m}|^2 = \frac{\sum_{i=0}^{L-1} \left|(-1)^{L-1-i} \cdot \sigma^{m+1}_{L-1-i,L-1}\right|^2}{\prod_{l=0,l\neq m}^{L-1}(\alpha_{m+1} - \alpha_{l+1})}. \tag{D-3}$$

Substituting $x = e^{-j\frac{2\pi}{L}k}$ in (C-4) results in the Discrete Fourier Transform of the sequence $\{(-1)^{L-1-i} \cdot \sigma^{m+1}_{L-1-i,L-1}\}_{i=0}^{L-1}$. Specifically,

$$\sum_{i=0}^{L-1}(-1)^{L-1-i} \cdot \sigma^{m+1}_{L-1-i,L-1} e^{-j\frac{2\pi}{L}ki} = \prod_{l=0,l\neq m}^{L-1} \left(e^{-j\frac{2\pi}{L}k} - \alpha_{l+1}\right), \quad k = 0, 1, \ldots, L-1, \tag{D-4}$$

from which the numerator of the expression in (D-3) can be calculated using Parseval relation and eq. (18) then follows.

APPENDIX E
OPTIMAL RECONSTRUCTION FILTERS

To find the filters $G_m(e^{j\omega})$ which minimize σ_e^2 in (6) under the constraints in (4), we use the Lagrange multipliers, where the Lagrangian is defined as

$$\mathcal{L}^{(i)} = \sum_{m=0}^{M-1} \sigma_m^2 \cdot |G_m(e^{j\omega})|^2 + \sum_{k=-i}^{L-1-i} \lambda_k^{(i)} \cdot \left(\sum_{m=0}^{M-1} G_m(e^{j\omega}) e^{-j\left(\omega - \frac{2\pi}{L}k\right)\frac{\tau_m}{T_N}} - L \cdot \delta[k]\right) \quad \omega \in \Delta\omega_i,\ i = 0, 1, \ldots, L-1. \tag{E-1}$$

Differentiating (E-1) with respect to $G_m^R(e^{j\omega}) = \Re(G_m(e^{j\omega}))$ and $G_m^I(e^{j\omega}) = \Im(G_m(e^{j\omega}))$, we obtain

$$\begin{aligned}
\frac{\partial \mathcal{L}^{(i)}}{\partial G_m^R(e^{j\omega})} &= 2\sigma_m^2 G_m^R(e^{j\omega}) + \sum_{k=-i}^{L-1-i} \Re(\lambda_k^{(i)}) \cdot \Re\left(e^{-j\left(\omega - \frac{2\pi}{L}k\right)\frac{\tau_m}{T_N}}\right) + \Im(\lambda_k^{(i)}) \cdot \Im\left(e^{-j\left(\omega - \frac{2\pi}{L}k\right)\frac{\tau_m}{T_N}}\right) \\
\frac{\partial \mathcal{L}^{(i)}}{\partial G_m^I(e^{j\omega})} &= 2\sigma_m^2 G_m^I(e^{j\omega}) + \sum_{k=-i}^{L-1-i} -\Re(\lambda_k^{(i)}) \cdot \Im\left(e^{-j\left(\omega - \frac{2\pi}{L}k\right)\frac{\tau_m}{T_N}}\right) + \Im(\lambda_k^{(i)}) \cdot \Re\left(e^{-j\left(\omega - \frac{2\pi}{L}k\right)\frac{\tau_m}{T_N}}\right) \\
&\quad \omega \in \Delta\omega_i,\ m = 0, 1, \ldots, M-1.
\end{aligned} \tag{E-2}$$

Solving (E-2) for $G_m(e^{j\omega})$ results in

$$G_m(e^{j\omega}) = 1/\sigma_m^2 \cdot e^{j\omega\tau_m/T_N} \left(\sum_{l=-i}^{L-1-i} \lambda_l^{(i)} \cdot e^{-j2\pi(\tau_m/LT_N)l}\right) \quad \omega \in \Delta\omega_i,\ i = 0, 1, \ldots, L-1,\ m = 0, 1, \ldots, M-1, \tag{E-3}$$

where the values of $\lambda_l^{(i)}$ are determined by the constraints in (4), i.e.,

$$\sum_{k=-i}^{L-1-i} \lambda_k^{(i)} \cdot \sum_{m=0}^{M-1} 1/\sigma_m^2 \cdot e^{-j\frac{2\pi}{L}(k-p)\frac{\tau_m}{T_N}} = L \cdot \delta[p], \quad p = -i, -i+1, \ldots, L-1-i, \quad i = 0, 1, \ldots, L-1. \tag{E-4}$$

REFERENCES

[1] W. C. Black and D. A. Hodges, "Time interleaved converter arrays," *IEEE J. Solid-State Circuits*, vol. SC-15, pp. 1022–1029, Dec 1980.

[2] J. L. Yen, "On nonuniform sampling of bandwidth-limited signals," *IRE Trans. Circuit Theory*, vol. 3, no. 4, pp. 251–257, 1956.

[3] Abdul J. Jerri, "The shannon sampling theorem - its various extensions and applications: A tutorial review," *Proceedings of the IEEE*, vol. 65, no. 11, pp. 1565–1596, 1977.

[4] A. Papoulis, "Generalized sampling expansion," *IEEE Trans. Circuits and Systems*, vol. CAS-24, no. 11, pp. 652–654, 1977.

[5] Y. C. Eldar and A. V. Oppenheim, "Filterbank reconstruction of bandlimited signals from nonuniform and generalized samples," *IEEE Trans. Signal Processing*, vol. 48, no. 10, pp. 2864–2875, 2000.

[6] Shay Maymon and Alan V. Oppenheim, "Quantization and compensation in sampled interleaved multi-channel systems," *Proceedings of ICASSP 2010, IEEE International Conference on Acoustics, Speech and Signal Processing*, March 2010.

[7] P. Marziliano and Martin Vetterli, "Reconstruction of irregularly sampled discrete-time bandlimited signal with unknown sampling locations," *IEEE Trans. Signal Processing*, vol. 48, no. 12, pp. 3462–3471, 2000.

[8] J. Elbornsson, F. Gustafsson, and J.-E. Eklund, "Blind adaptive equalization of mismatch errors in time-interleaved a/d converter system," *IEEE Trans. Circuits Syst.*, vol. 51, no. 1, pp. 151–158, 2004.

[9] M. Seo, M. J. W. Rodwell, and U. Madhow, "Blind correction of gain and timing mismatches for a two-channel time-interleaved analog-to digital converter," *Proc. 39th Asilomar Conf. Signals, Syst.*, p. 11211125, 2005.

[10] S. Huang and B. C. Levy, "Adaptive blind calibration of timing offset and gain mismatch for two-channel time-interleaved adcs," *IEEE Trans. Circuits Syst.*, vol. 53, no. 6, pp. 12781288, 2006.

[11] C. Vogel, "A frequency domain method for blind identification of timing mismatches in time-interleaved adcs," *Proc. Norchip Conf.*, pp. 45–48, 2006.

[12] S. Huang and B. C. Levy, "Blind calibration of timing offsets for four channel time-interleaved adcs," *IEEE Trans. Circuits Syst.*, vol. 54, no. 4, pp. 863876, 2007.

[13] T. Strohmer and J. Xu, "Fast algorithms for blind calibration in time interleaved analog-to-digital converters," *Proc. IEEE ICASSP*, p. 12251228, 2007.

[14] Vijay Divi and Gregory W. Wornell, "Blind calibration of timing skew in time-interleaved analog-to-digital converters," *IEEE Journal of Selected Topics in Signal Processing*, vol. 3, no. 3, pp. 509, 2009.

[15] Y. C. Jenq, "Digital spectra of nonuniformly sampled signals: a robust sampling time offset estimation algorithm for ultra high-speed waveform digitizers using interleaving," *IEEE Trans. Instrum. Meas.*, vol. 39, no. 1, pp. 71–75, 1990.

[16] H. Jin and E. K. F. Lee, "A digital-background calibration technique for minimizing timing-error effects in time-interleaved adcs," *IEEE Trans. Circuits Syst.*, vol. 47, no. 4, pp. 603–613, 2000.

[17] Alan V. Oppenheim and Ronald W. Schafer, *Discrete-Time Signal Processing*, Prentice Hall, 2010.

[18] J.C. Candy and G.C. Temes, *Oversampling Delta-Sigma Data Converters*, IEEE Press New York, NY, 1992.

[19] Ramin Khoini-Poorfard and David A. Johns, "Time-interleaved oversampling convertors," *Electronics Letters*, vol. 29, no. 19, pp. 1673 – 1674, 2002.

[20] Ramin Khoini-Poorfard, Lysander B. Lim, and David A. Johns, "Time-interleaved oversampling a/d converters: Theory and practice," *IEEE Trans. Circuits and Systems*, vol. 44, no. 8, pp. 634–645, 1997.

[21] Nguyen T. Thao and Martin Vetterli, "Lower bound on the mean-squared error in oversampled quantization of periodic

signals using vector quantization analysis," *IEEE Trans. Information Theory*, vol. 42, no. 2, pp. 469–479, 1996.

[22] C.Y. Ho, Bingo Wing-Kuen Ling, and J.D. Reiss, "Noise analysis of modulated quantizer based on oversampled signals," *ICASSP 2006 Proceedings*, pp. 728–731, 14-19 May 2006.

[23] R. E. Crochiere, S. A. Webber, and J. L. Flanagan, "Digital coding of speech in sub-bands," *Bell System Technical Journal*, vol. 55, no. 8, pp. 10691085, 1976.

[24] Lawrence Rabiner and Ronald Schafer, *Theory and Applications of Digital Speech Processing*, Prentice Hall, 2010.

[25] M. Vetterli, J. Kovačević, and V. K. Goyal, *Fourier and Wavelet Signal Processing*, 2011, Release α2.0 available online at `http://FourierAndWavelets.org`.

[26] W.R. Bennett, "Spectra of quantized signals," *Bell System Technical J.*, vol. 27, pp. 446–472, 1948.

[27] Anekal B. Sripad and Donald L. Snyder, "A necessary and sufficient condition for quantization errors to be uniform and white," *IEEE Trans. Acoustics, Speech, and Signal Processing*, vol. ASSP-25, no. 5, pp. 442–448, 1977.

[28] Bernard Widrow, Istvan Kollar, and Ming Chang Liu, "Statistical theory of quantization," *IEEE Trans. Instrumentation and Measurement*, vol. 45, no. 2, pp. 353–361, 1996.

[29] Bernard Widrow and Istvn Kollr, *Quantization Noise: Roundoff Error in Digital Computation, Signal Processing, Control, and Communications*, Cambridge University Press, 2008.

[30] Shay Maymon, ," *Ph.D. dissertation, Mass. Inst. of Technology, Cambridge, MA*, 2011.

[31] Max A. Woodbury, "Inverting modified matrices," *Memorandum Rept. 42, Statistical Research Group, Princeton University, Princeton, NJ*, 1950.

[32] N. Macon and A. Spitzbart, "Inverses of vandermonde matrices," *The American Mathematical Monthly*, vol. 65, no. 2, pp. 95–100, 1958.